

# CHEMISTRY

---

## AN ASIAN JOURNAL

www.chemasianj.org

### Accepted Article

**Title:** Board-like Fused-Thiophene Liquid Crystals and Their Benzene Analogues: Facile Synthesis, Self-assembly, p-Type Semiconductivity, and Photoluminescence

**Authors:** Bertrand Donnio, Kai Chun Zhao, Jun Qi Du, Hai Feng Wang, Ke Qing Zhao, Ping Hu, Bi Qin Wang, Hirosato Monobe, and Benoît Heinrich

This manuscript has been accepted after peer review and appears as an Accepted Article online prior to editing, proofing, and formal publication of the final Version of Record (VoR). This work is currently citable by using the Digital Object Identifier (DOI) given below. The VoR will be published online in Early View as soon as possible and may be different to this Accepted Article as a result of editing. Readers should obtain the VoR from the journal website shown below when it is published to ensure accuracy of information. The authors are responsible for the content of this Accepted Article.

**To be cited as:** *Chem. Asian J.* 10.1002/asia.201801483

**Link to VoR:** <http://dx.doi.org/10.1002/asia.201801483>

A Journal of



A sister journal of *Angewandte Chemie*  
and *Chemistry – A European Journal*

---

WILEY-VCH

# Board-like Fused-Thiophene Liquid Crystals and Their Benzene Analogues: Facile Synthesis, Self-assembly, p-Type Semiconductivity, and Photoluminescence

Kai-Chun Zhao,<sup>[a]</sup> Jun-Qi Du,<sup>[a]</sup> Hai-Feng Wang,<sup>[a]</sup> Ke-Qing Zhao,<sup>\*[a]</sup> Ping Hu,<sup>[a]</sup> Bi-Qin Wang,<sup>[a]</sup> Hirosato Monobe,<sup>\*[b]</sup> Benoît Heinrich,<sup>[c]</sup> and Bertrand Donnio<sup>\*[c]</sup>

**Abstract:** Novel fused-thiophene discotic liquid crystals were designed and easily synthesized by Suzuki coupling and FeCl<sub>3</sub> oxidized tandem cyclo-dehydrogenation reactions, including homo- and cross-coupling reactions. The resulting hexagonal and rectangular columnar mesomorphic supramolecular structures formed were characterized by polarizing optical microscopy, differential scanning calorimetry, and small-angle X-ray scattering. Charge carrier transport properties in the mesophases of two of the synthesized fused-thiophene discogens were measured by transient photocurrent time-of-flight (TOF) technique, revealing fast hole transport values in the range of 10<sup>-3</sup> to 10<sup>-2</sup> cm<sup>2</sup> V<sup>-1</sup>s<sup>-1</sup>, thus demonstrating potential applications in electronic devices. The luminescent sanidic mesogens, having different extended  $\pi$ -conjugated systems, also emit blue, green or red light, with absolute photoluminescent quantum yields as high as 18%.

## Introduction

Thiophene-containing  $\pi$ -conjugated aromatics [1,2] and polythiophene derivatives [3,4] are important basic molecular components of organic semiconductors. Polythiophenes as polymeric semiconductors become electrical conductors when doped: poly(3,4-ethylenedioxythiophene) (PEDOT) doped with polystyrene sulfuric acid becomes conjugated conducting

polymer and plays a key role in plastic electronics.[5] while poly-3-hexylthiophene (P3HT) as a p-type organic semiconductors when paired with the n-type C<sub>60</sub> fullerene derivatives exhibits superior performance in organic photovoltaic solar cells.[6] Oligothiophene derivatives end-capped with alkyl chains, show liquid crystalline properties,[7-20] and prefer to self-organize into supramolecular ordered layered structures: they display two-dimensional charge transport mobility comparable to inorganic semiconductors of amorphous and polycrystalline silicon, and have been investigated as active materials in organic field-effect transistors (OFET).[21-25] Discotic liquid crystals (DLCs) [26-29] which contain a fused-thiophene unit [30-46] are also attractive candidates as novel organic semiconductors due to their advantageous combination of the highly applicable and promising electronic properties of the thiophene moiety and the propensity of DLCs to self-organize into columnar mesophase for one-dimensional charge transport pathways.[26] However, the number of thiophene-containing DLCs is still limited compared to the numerous rod-like liquid crystals incorporating a thiophene unit. We report here the design and synthesis of such discotic systems by combined Suzuki and Scholl coupling reactions. Novel molecular design, supported by facile and efficient synthetic strategies for the construction of thiophene-fused DLCs are highly desirable for the discovery of new materials and for modulating the applicable physical properties. Here, a simple, direct and highly efficient synthetic route for the preparation of novel fused-thiophene DLCs by (cross) oxidative cyclodehydrogenation is reported (**5-8**, Scheme 1). This route was used in parallel for the preparation of the benzene and biphenylene analogues (**9-10**, Scheme 2). The mesomorphism and thermal behavior of all the compounds were characterized by polarizing optical microscopy (POM), differential scanning calorimetry (DSC), and small-angle X-ray scattering (SAXS), and the self-organizational behavior of the two series of dumbbell-shaped discotic compounds, with half-disc-like mesogens either rigidly joined by fused rings (compounds **5**, **7** and **9**), or connected by a sigma bond through fused ring extenders (compounds **6**, **8** and **10**) was compared. The molecular structure-mesomorphism relationship is discussed and the unique effect of thiophene on the mesomorphism is stressed. Furthermore, this synthetic strategy was successfully extended to the synthesis of a novel unsymmetrical discogen **11**, and is also described (Scheme 3). Semiconductive property measured by photocurrent time-of-flight technique are also reported for two representative compounds, namely a discotic columnar mesogen (**5**) and a discotic dimer (**6**), revealing rather high, one-dimensional charge carrier mobility in

- [a] Mr K.-C. Zhao, Mr J.-Q. Du, Mr H.-F. Wang, Prof K.-Q. Zhao\*, Prof P. Hu and Prof B.-Q. Wang  
College of Chemistry and Materials Science,  
Sichuan Normal University  
Chengdu 610066, China  
E-mail: kqzhao@sicnu.edu.cn
- [b] Prof H. Monobe\*  
Inorganic Functional Materials Research Institute  
National Institute of Advanced Industrial Science and Technology  
(AIST)  
Ikeda, Osaka 563-8577, Japan  
E-mail: monobe-hirosato@aist.go.jp
- [c] Dr B. Heinrich and Dr B. Donnio\*  
Institut de Physique et Chimie des Matériaux de Strasbourg  
(IPCMS)  
CNRS-University de Strasbourg (UMR 7504)  
23 rue du Loess, BP43 67034 Strasbourg, Cedex 2, France  
E-mail: bertrand.donnio@ipcms.unistra.fr

Supporting information for this article is given via a link at the end of the document.

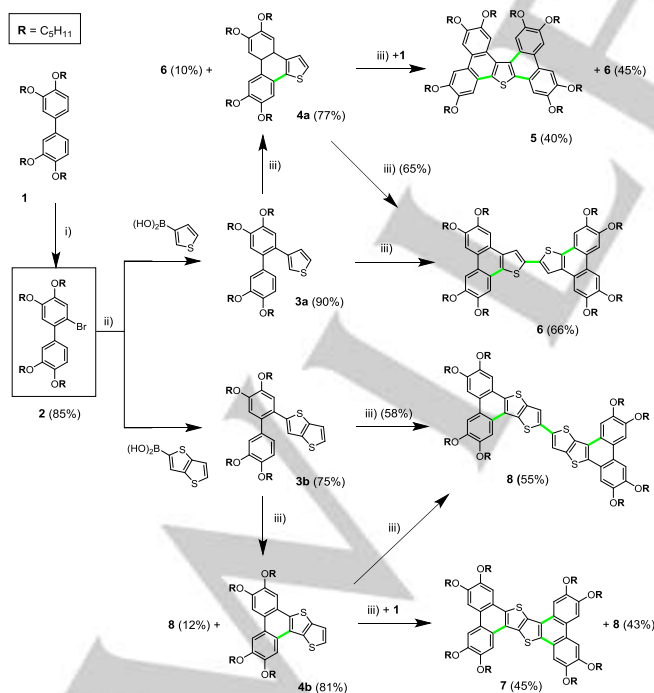
## FULL PAPER

the range of  $10^{-3}$ – $10^{-2}$   $\text{cm}^2 \text{V}^{-1} \text{s}^{-1}$ . These sanidic mesogens are also luminescent and emit blue, green or red light, with absolute photoluminescent quantum yields as high as 18%.

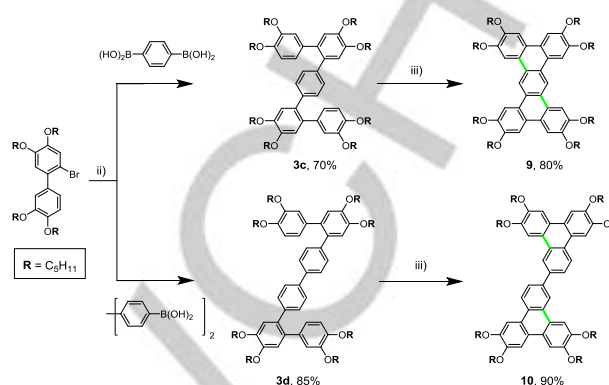
## Results and Discussion

**Synthesis and characterization.** The key compound for this synthesis is 2-bromo-3',4,4',5-tetrakis(pentyloxy)-1,1'-biphenyl (**2**, Schemes 1 and 2), which is readily obtained in good yield (> 85%) from the bromination of 3,3',4,4'-tetrakis(pentyloxy)-1,1'-biphenyl, **1**, in one step, as already reported previously.[47] Running the reaction above  $-5^\circ\text{C}$  or using excess liquid bromine resulted in dibromination of the biphenyl, reducing substantially the yield of **2** and making purification by column chromatography more difficult. Palladium-catalyzed Suzuki cross-coupling reaction of various arylboronic acids (e.g. thiophene-3-boronic acid, thieno[3,2-b]thiophene-2-boronic acid, 1,4-phenyldiboronic acid, 4,4'-biphenylboronic acid) with **2** was first applied to produce the corresponding mono-substituted compounds **3a-d** in yields of 70–90 % (Schemes 1 and 2, respectively).

Then, oxidative cyclodehydrogenation of **3a-d** was followed, for which the amount of oxidizing agent,  $\text{FeCl}_3$ , was found to crucially affect the reaction yields. The amount of  $\text{FeCl}_3$  used was actually determined by the number of C-C bond formed and hydrogen atoms eliminated: for each C-C bond formation, two H-atoms were eliminated, and two equiv.  $\text{FeCl}_3$  were used. The solution of  $\text{FeCl}_3$  (50 mg) in  $\text{CH}_3\text{NO}_2$  (0.5 mL) was prepared before use, and the substrates were dissolved in  $\text{CHCl}_3$  or  $\text{CH}_2\text{Cl}_2$ . The reactions, monitored by thin-layer chromatography, were completed in 1 h at room temperature.



**Scheme 1.** Synthesis of fused-thiophene and dimeric discogens **5-8**: i)  $\text{Br}_2$ ,  $\text{CH}_2\text{Cl}_2$ ,  $0^\circ\text{C}$ ; ii)  $\text{Pd}(\text{PPh}_3)_4$ ,  $\text{K}_2\text{CO}_3$ ,  $\text{H}_2\text{O}/\text{THF}$ ,  $80^\circ\text{C}$ ; iii)  $\text{FeCl}_3$ ,  $\text{MeNO}_2/\text{CH}_2\text{Cl}_2$ , RT.



**Scheme 2.** Synthesis of  $\pi$ -extended discogen **9** and triphenylene dimer **10**: ii)  $\text{Pd}(\text{PPh}_3)_4$ ,  $\text{K}_2\text{CO}_3$ ,  $\text{H}_2\text{O}/\text{THF}$ ,  $80^\circ\text{C}$ ; iii)  $\text{FeCl}_3$ ,  $\text{MeNO}_2/\text{CH}_2\text{Cl}_2$ , RT.

The intermediates **4a** and **4b** were prepared by the intramolecular Scholl reaction of **3a** and **3b** with 2 equiv. of  $\text{FeCl}_3$  at room temperature, in yields of 77 % and 81 %, respectively, along with the formation of small amounts of dimeric products, **6** and **8** (Scheme 1). Excess  $\text{FeCl}_3$  or running the reaction longer time resulted in decreased yields. Intermolecular oxidative cross-coupling reactions of **4a** and **4b** in the presence of the biphenyl derivative **1** produced **5** and **7**, respectively. In this reaction, the substrate ratio of fused-thiophene (**4a** and **4b**) with biphenyl **1** was 1:1, and four equiv. of  $\text{FeCl}_3$  were used. Production of dimeric compounds **6** and **8** was also observed, both oxidative cross-coupling and homo-coupling reactions being in competition as the  $\alpha$ -position of the (fused) thiophene is also more reactive. As the homo-coupled products **6** and **8** are less soluble than the cross-coupled products **5** and **7**, increasing the solvent was found to favor the formation of the former (**5** and **7**). When the amount of  $\text{FeCl}_3$  was lowered, the oxidative dimerization products **6** and **8** was promoted over the intermolecular coupling, and compounds **5** and **7** were obtained with yields of 40% and 45%, respectively, whereas dimers **6** and **8** were formed simultaneously with similar yields of 45% and 43%, respectively. Thus, the overall transformations of **4a** and **4b** are higher than 80%. Note that the direct coupling of **3a** and **3b** with biphenyl **1** also produced **5** and **7**, but in yields lower than 5%, whereas when more than 6 equiv. of  $\text{FeCl}_3$  were used, **6** and **8** were obtained as the major products. Compounds **6** and **8** were synthesized by the direct oxidative homo-coupling of **4a** and **4b** with 2 equiv. of  $\text{FeCl}_3$  in 65% and 55% yields, respectively. The most efficient transformation of **3a** and **3b** to **6** and **8** (66% and 58%, respectively) was achieved by tandem intra- and inter-molecular coupling reactions with 4 equiv. of  $\text{FeCl}_3$ .

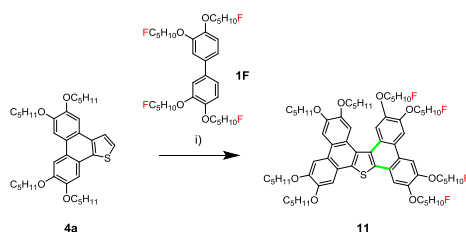
Similarly, compounds **9** and **10** were directly prepared by the  $\text{FeCl}_3$  (4 equiv.) oxidative cyclodehydrogenation of **3c** and **3d**, respectively. After the reaction was finished, **9** and **10** precipitated from the solution as white powders, due to the decreased solubility in organic solvents as compared to the starting

For internal use, please do not delete. Submitted\_Manuscript

## FULL PAPER

compounds **3c** and **3d**. Pure regioisomers **9** and **10** were isolated in good yields (80 and 90%, respectively) after filtration and abundant washing with water, de-coloring by active carbon and recrystallization.

The strategy used for the preparation of **5** suggested the possibility to also prepare related unsymmetrical discogenic compounds, with two edges of different chemical natures. We successfully tested this possibility by reacting **4a** with another biphenylene derivative (**1F**, Scheme 3) through the tandem intramolecular and intermolecular Scholl reaction. Without optimizing the synthetic conditions, compound **11** was prepared in moderate yields, ca. 34%, showing the great potential of this tandem reaction to be exploited for the design of a large range of novel types of Janus compounds, with modified and adapted properties, such as solubility, wettability, self-organization, phase transition temperatures, of both fundamental and applied interests.



**Scheme 3.** One-pot synthesis of low-symmetry discogen **11** by tandem intramolecular and intermolecular Scholl reaction. i)  $\text{FeCl}_3$ ,  $\text{CH}_2\text{Cl}_2$ ,  $\text{MeNO}_2$ .

All the intermediates, and the target compounds have been fully characterized by NMR (Figures S1-14) and HRMS (Figures S15-21), and the results are in good agreement of the chemical structures. No positional isomers were observed, otherwise different from the reported phenomena.[48]

**Molecular conformation and aggregation in organic solvents.** Polycyclic aromatic hydrocarbons usually tend to aggregate in organic solvents due to strong intermolecular interactions, which depend essentially on the size and planarity of the aromatic core. The synthesized fused thiophene discotic compounds described here possess these features and therefore were expected to strongly aggregate in solution.

The aggregation behavior in solution of compounds **5**, **6** and **8**, has been examined by  $^1\text{H}$  NMR, and their concentration-dependent spectra are shown in Figure 1 (and Figure S22). The strong tendency for the aggregation behavior is evidenced in spectra of compounds **6** and **8**: as the concentration of **6** or **8** in  $\text{C}_6\text{D}_6$  increases (from 5 to 15 mg/mL), the chemical shift values of the aromatic protons move to upper field with lower value of chemical shift value; for **8** this tendency is even stronger, as the proton signals become broadened and unresolved (Figure S22). In contrast, compound **5** in  $\text{CDCl}_3$  shows no aggregation behavior in solution, as evidenced by the invariance of the  $^1\text{H}$  NMR spectra aromatic signals with increasing of the concentration (Figure 1). These observations are in agreement with the molecular structures of the compounds: **6** and **8** both have a similar structure that consists of a sigma-bond connecting two discotic fused flat

aromatic cores into a twin extended structure which can easily stack, whereas **5**, although possesses a fused aromatic core, but due to the presence of the meta alkoxy chains pointing towards the cavity, has a non-planar, twisted core and therefore presents weaker  $\pi$ - $\pi$  intermolecular interactions. The most stable molecular conformations of **5** ~ **8** calculated by density functional theory (B3LYP-D3/6-311+\*\*), shown in Tables S1-2, further support these experimental results. The DFT calculated molecular structures show that the single aromatic core of **5** is indeed not flat, while for dimers **6** and **8**, the two aromatic cores connected through a sigma-bond, are in contrast planar. Although the dimeric molecules may not be planar, the flexibility of the sigma bond allows stacking of the constitutive flat cores in solution due to the favourable face-to-face  $\pi$ - $\pi$  interactions. The shift and broadening of their  $^1\text{H}$  NMR signals is likely the signature of the aggregation of **6** and **8** in solution, as observed frequently for other polycyclic aromatic hydrocarbons (PAHs).

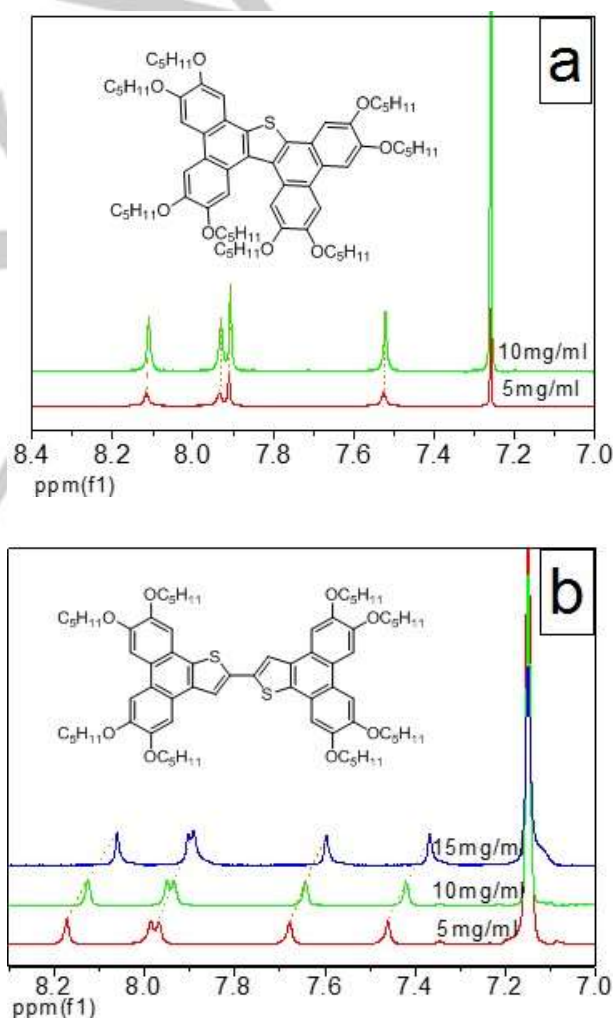


**Figure 1.** Aromatic region of the  $^1\text{H}$  NMR spectra at different concentrations of compound: (a) **5** in  $\text{CDCl}_3$ , (b) **6** in  $\text{C}_6\text{D}_6$ .

For internal use, please do not delete. Submitted\_Manuscript

## FULL PAPER

**Thermal behavior by DSC and POM.** The liquid crystalline properties of the final compounds (**5-11**) were investigated first by POM (Figures 2 and S23) and DSC (Figure S24, DSC data gathered in Table 1). All samples were observed under optical polarizing microscope with a heating-stage, and when slowly cooled from their isotropic liquid states, exhibited fluid and birefringent optical textures reminiscent of columnar liquid-crystalline phases (Figure 2): fan-shaped textures typical of columnar textures with strong homeotropic alignment were observed for **5-7** and **9-11**. **8** behaved differently, and first showed a schlieren texture characteristic of a nematic phase, which changed to columnar-like texture with edge-on orientation on further cooling. Consistently with the extended  $\pi$ -conjugated, overall sanidic-like structures of the compounds, the mesomorphism in this series is *a priori* dominated by the formation of columnar phases. Except compounds **5** and **11** that possess a distorted non-planar structure (Table S1) and melt at 110-117°C, all the other mesogens possess rather high transition temperatures, with melting in the range between ca. 180 and 220°C. Mesogens **7** and **9**, which have the most co-planar aromatic core structure, and likely stronger  $\pi$ - $\pi$  intermolecular interactions, exhibit the highest clearing (ca. 310 and 280°C, respectively) and the largest mesomorphic temperature range (120 and 60°C, respectively). The  $\sigma$ -bridge between both the two protomesogenic units in dimers **8** and **6**, results in the reduction of the clearing temperature, concomitantly to that of the mesomorphic range (55 and 43°C, respectively), whereas the less hindered rotation in dimer **10** results in the complete destabilization of the mesomorphism, yielding a narrow, metastable monotropic rectangular columnar phase. Quite unexpected, the unsymmetrical compound (**11**) exhibits a monotropic phase (identified as Col<sub>hex</sub> by POM, Figure 2), which is very different to the behavior of its structurally related symmetrical homologue compound (**5**): although both have similar melting temperatures (114 vs. 117°C), they possessed very different clearing temperatures (134 vs. 74°C). Differential scanning calorimetry (DSC, Figure S24) results confirmed POM observations. Recall that intermediates **3a-d**, **4a** and **4b** did not show mesophase, directly melting when heated into the isotropic liquid, and crystallizing when cooled with some supercooling.

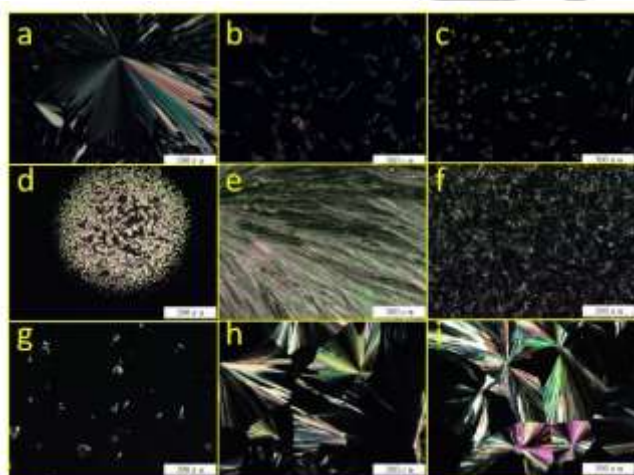


**Figure 2.** POM images of the discotic liquid crystals on slow cooling from the isotropic liquid (of: (a) **5** at 121°C, (b) **6** at 230°C, (c) **7** at 258°C, (d) **8** at 265°C, (e) **8** at 229°C, (f) **9** at 262°C, (g) **10** at 165°C, (h) and (i) **11** at 104 and 90°C, fan-shaped textures with homeotropic domains for columnar phase, and schlieren texture for the nematic phase (Additional POM images are shown in Figure S23).

**Table 1.** Phase transition temperatures (°C) and enthalpy changes ( $\Delta H$ , kJ mol<sup>-1</sup>) of board-like mesogenic compounds (measured by DSC at 10°C/min heating/cooling rate).<sup>[a]</sup>

	2 <sup>nd</sup> Heating	1 <sup>st</sup> Cooling
<b>5</b>	Cr 68.4 (-33.4) Cr' 102.4 (7.7) Cr'' 114.2 (52.2) Col <sub>hex</sub> 134.4 (9.3) Iso	Iso 133.9 (-9.3) Col <sub>hex</sub> 69.1 (-3.4) Cr
<b>6</b>	Cr 22.4 (3.1) Cr' 95.5 (9.5) Cr'' 119.4 (8.1) Cr''' 189.2 (34.3) Col <sub>rec</sub> 232.7 (4.7) Iso	Iso 231.4 (-4.4) Col <sub>rec</sub> 182.1 (-28.8) Cr''' 165.6 (-5.5) Cr'' 107.4 (-7.3) Cr' 11.7 (-2.1) Cr
<b>7</b>	Cr 114.8 (4.2) Cr' 146.2 (-) <sup>[b]</sup> Cr'' 177.4 (24.6) Cr''' 188.4 (-) <sup>[b]</sup> Col <sub>hex</sub> 307.2 (8.5) Iso	Iso 306.7 (-6.4) Col <sub>hex</sub> 162.0 (-23.7) Cr' 92.7 (-10.9) Cr
<b>8</b>	Cr 206.7 (49.7) Cr' 213.3 (4.4) Col <sub>rec</sub> 263.9 (4.7) N 268.8 (0.9) Iso	Iso 268.8 (-1.0) N 262.3 (-4.9) Col <sub>rec</sub> 152.0 (-47.5) Cr
<b>9</b>	Cr 145.5 (20.9) Cr' 222.1 (49.2) Col <sub>hex</sub> 281.0 (9.2) Iso	Iso 280.8 (-9.1) Col <sub>hex</sub> 215.9 (-52.4) Cr' 135.1 (-17.3) Cr
<b>10</b>	Cr 183.7 (65.4) Iso	Iso 169.5 (-54.8) Col <sub>rec</sub> 157.8 (-4.0) Cr
<b>11</b>	Cr 88 (-38.9) Cr' 117 (70.4) Iso	Iso 106 (-6.7) Col <sub>hex</sub> 74 (-17.3) Cr

[a] Cr-Cr''': crystalline solids; Col<sub>hex</sub>: columnar hexagonal mesophase; Col<sub>rec</sub>: columnar rectangular mesophase; N: nematic phase; Iso: isotropic liquid. \*Cumulated enthalpy. [b] Cumulated enthalpies.

**Characterization of the mesophases by small angle X-ray scattering (SAXS).** The SAXS patterns were recorded for all compounds but **11**, at various temperatures (Figures 3 and S25, Tables 2 and S3). They give patterns exhibiting the characteristic signals of columnar mesophases, namely the scattering signals,  $h_{ch}$  and  $h_{\pi}$ , emerging from lateral distances between molten chains and stacking distances of mesogens, and the sharp reflections ( $hk$ ) from the two-dimensional arrangement of the mesogenic columns separated in space by molten aliphatic continuum. The presence of additional broad signals at small and intermediate angular range, D1 and D2, was also detected, which were associated to correlation lengths between 4 and 10 nm, and evidenced the development of a local-range three-dimensional superstructure between individual mesogens. The mesophase of the series with fused rings bridges (**5**, **7**, **9** and by extension to **11**) was logically found to be columnar hexagonal, Col<sub>hex</sub>, since the mesogens come down to a unique pseudo discoid platform with moreover an aspect ratio  $q_{ch}$  not far from unity (Table 2).[49,50] These features allow easy orientational changes of stacked

For internal use, please do not delete. Submitted\_Manuscript

## FULL PAPER

mesogens within and between columns, which equally distribute the aliphatic chains in the periphery of the columns. Corollary, the cross-section of the columns is averaged to a cylinder and the symmetry of the lattice is augmented to hexagonal. In addition, various mechanisms, such as the tilting of the mesogens inside columns, compensate for the discrepancy between the column envelope area and the space requirement of peripheral chains. Along this line, the tilt angles found for the three compounds range from 23 to 37°, for interface areas per alkyl chain overcoming slightly the cross sectional area of a fully stretched chain (the ratios  $q_{ch}$  range from 1.019 to 1.065, Table 2). The molecular organization is driven by the optimal nanosegregation between mesogenic cores and aliphatic periphery and is thus essentially the same for the three compounds. As a matter of fact, compounds mostly differ by the extensions of the  $Col_{hex}$  phase, as it exists in broad range, up to high temperatures, for the thienothiophene or the phenyl bridges, but restricts to a narrow range located at relatively low temperature for the thiophene bridge. The reason is obviously that the mesogen is not really dumbbell-shaped in this latter case and that the alkyl substituents connected to the closely spaced phenanthrene segments interfere in a detrimental manner with the regular face-to-face stacking into columns.

For the series with the bridges including a sigma bond, the mesophase was found to be  $Col_{rec}$  for **6** and **8**, and the same very likely applies to **10**, although its mesomorphic range is limited to a narrow monotropic one, which prevented the acquisition of a conclusive SAXS pattern. Unlike the precedent rigid bridges, these ones authorize rotation around the bond axis and hence preserve the individuality of both mesogen halves, besides of being longer and thus combining with higher aspect ratios. These features hamper the orientation changes along the piles of  $\pi$ -stacked mesogens and thus naturally lead to columns with an elongated cross-section that arrange in a columnar phase of lower symmetry. Specifically, the cross-sections of columns were found to align in the same direction, defining the  $a$ -axis of a rectangular  $c2mm$  lattice. Again, the main difference between compounds lies in the extension of the mesomorphic domains, with in particular broad ranges persisting at high temperatures for **6** and **8**, and only a narrow monotropic phase in combination with a low clearing temperature for **10**. Focusing first on **10** and **6**, whose connecting bridges (i.e. biphenyl and bistiophene) have comparable lengths, the huge variations of the mesomorphic properties observed could not be explained by the influence of the sole chemical nature on the lateral interactions. Both bridges have however different orientations of the terminal fused ring edge, so that the phenanthrene segments pend aside for biphenyl or are in line with the bridge for bistiophene. This leads to a true dumbbell-shaped geometry for the bistiophene that promotes a regular face-to-face stacking with an equal surrounding of aliphatic tails. To reach the same configuration with the phenanthrene segments and thus the alkyl substituents pending aside, neighboring mesogens have to shift and/or to change orientation along piles. This might be the main origin of the early clearing transition of **10**. Accordingly, the mesogen geometry would also have a detrimental effect for **8**, despite that the contribution of the extended bridge to the cohesion of the self-assembling would however counterbalance.

At last, **8** exhibits a broad  $Col_{rec}$  range at even higher temperature than **6**, but the change of geometry is nevertheless reflected in the appearance of a 30-40° tilting inside columns and the related lattice shrinking along  $b$ -axis, whereas **6** self-organizes in untilted columns.

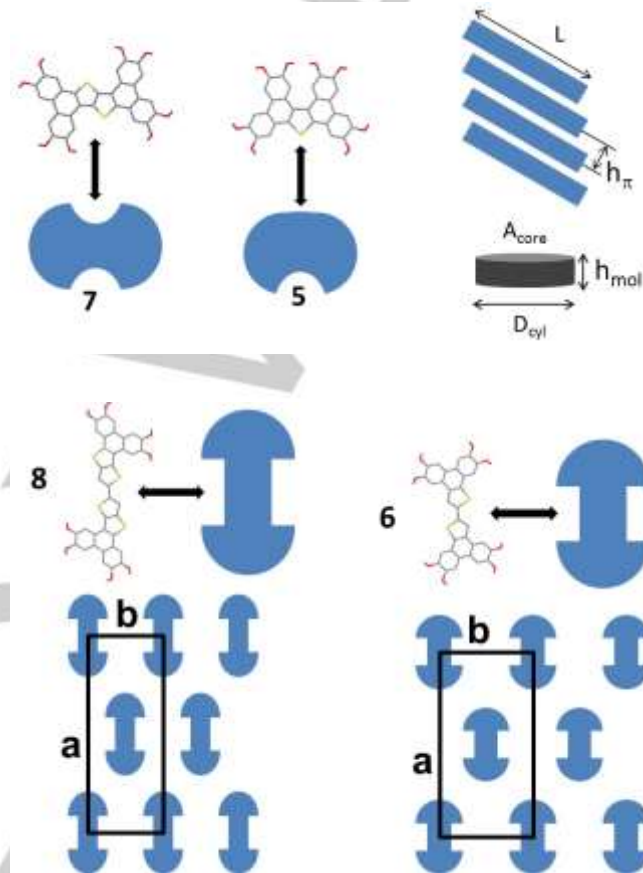


**Figure 3.** Supramolecular model. Fused core terms **7**, **5** and **9** (and **11**) self-organize in a  $Col_{hex}$  mesophase, with the mesogens stacked into tilted columns, whose cross-section is averaged to a cylinder. Fused core members **8** and **6** self-organize in a  $Col_{rec}$  mesophase, for which the dumbbell-shaped columns of stacked mesogens are arranged in a rectangular  $c2mm$  lattice ( $Z = 2$ ). The electronic density distribution resulting from this particular column shape explains the high intensity difference of fundamental reflections (20) and (11). Along columns, the stacking is either tilted ( $\psi=30-40^\circ$ ) for **8** or untilted for **6**. The mesophase type and the arrangement are likely the same for **10**.

**Table 2.** Geometrical mesophases parameters.<sup>[a]</sup>

Phase T		$V_{mol}$ $\rho$ $\chi V_{ch}$	$a$ $b$ $A[Z]$	$h_{mol}$ $h_{\pi}$	$\psi$	$A_{core}$ $D_{cyl}$	$S_{ch,cyl}$ $q_{ch,cyl}$
<b>7</b>	$Col_{hex}$	2021	23.48	4.23	28	181	25.2
	240	0.93	-	3.74		15.2	1.019
		0.622	477[1]				
<b>5</b>	$Col_{hex}$	1825	22.48	4.17	23	160	23.4

For internal use, please do not delete. Submitted\_Manuscript

## FULL PAPER

	120	0.98 0.88	- 438[1]	3.83		14.3	1.023
<b>9</b>	Col <sub>hex</sub> 250	2008 0.88 0.63	21.94 - 417[1]	4.82 3.82	37	154 14.0	26.5 1.065
<b>8</b>	Col <sub>rec</sub> 240	2169 0.97 0.579	50.40 19.25 971[2]	4.47 3.62	36	- -	- -
<b>6</b>	Col <sub>rec</sub> 210	2043 0.94 0.604	47.30 23.96 1133[2]	3.60 3.65	0	- -	- -
<b>10*</b>	Col <sub>rec</sub> 165	2011 0.94 0.595	51.28 22.86 1172[2]	3.43 3.68	0	- -	- -

[a] Mesophase, T, temperature of the measurement (°C);  $V_{mol}$ , molecular volume ( $\text{\AA}^3$ );  $\rho$ , density ( $\text{g cm}^{-3}$ ) calculated from partial volumes of reference substances (accuracy ca. 4%);  $\chi_{V, ch}$ , aliphatic volume fraction ( $\chi_{V, ch} = V_{ch}/V_{mol}$ );  $a$ ,  $b$ , lattice parameters ( $\text{\AA}$ );  $A$ , area (Col<sub>hex</sub>:  $A = 2a^2/\sqrt{3}$ ; Col<sub>rec</sub>:  $A = axb$ ;  $\text{\AA}^2$ );  $Z$ , number of columns per lattice;  $h_{mol}$ , columnar slice thickness ( $\text{\AA}$ ),  $h_{mol} = V_{mol}/(Z \times A)$ ;  $h_{\pi}$ , stacking distance from SAXS pattern;  $\psi$ , out-of-plane tilt angle of mesogens inside columns,  $\psi = \arccos(h_{\pi}/h_{mol})$  (°);  $A_{core}$ , cross-sectional area of columnar cores ( $\text{\AA}^2$ ),  $A_{core} = \chi_{V, ch} A/Z$ ;  $D_{cyl}$  ( $\text{\AA}$ ), diameter of equivalent cylinder of cross-sectional area  $A_{core}$ ;  $S_{ch, cyl}$ , cylinder area per chain ( $\text{\AA}^2$ ),  $S_{ch, cyl} = \pi D_{cyl} h_{mol}/n_{ch}$ ,  $n_{ch}$  being the number of chains per molecule ( $n_{ch} = 8$ );  $q_{ch, cyl}$ , chain packing ratio,  $q_{ch, cyl} = S_{ch, cyl}/\sigma_{ch}$ ,  $\sigma_{ch}$  being the cross-sectional area of a molten chain. (\*) The mesophase being monotropic, SAXS acquisition time was limited, leading to some measurement uncertainties.

**Charge carrier mobility by time-of-flight (TOF) technique.** Columnar discotic liquid crystals possessing polycyclic aromatic core are well known as mesophase semiconductors,[51-55] the discotic column formed by the stacked aromatic cores functioning as electron transport pathway with one-dimensional feature of molecular wire, while the peripheral alkyl chains serve as insulators. DLC semiconductors are presently investigated as active materials in printed organic thin-film devices, such as organic photovoltaic solar cells (OPV),[56] organic field-effect transistors (OFET),[26] and organic light-emitting diodes (OLED).[27] Intrinsic charge carrier mobility is an important parameter for mesophase semiconductors. The electronic transport data can be obtained by different techniques, such as thin-film field-effect transistors, pulse radiolysis time-resolved microwave conductivity (PR-TRMC), photocurrent time-of-flight technique (TOF). TOF technique gives directly reliable hole and electron mobility, and is suitable for the investigation of the semiconducting property of columnar liquid crystals, with homeotropic orientation of the samples between the ITO cells, and sample thickness of 10~20  $\mu\text{m}$ , similar to the thickness of standard electronic devices.

Both discogens **5** and **6** were selected for the measurement of the charge drift mobility rates. Actually, they exhibited the lowest isotropization temperatures within the series, making them suitable for filling the samples cells by capillary force in their isotropic liquid state. Both **5** and **6** display non-dispersive photocurrent decay curves (Figures 4 and 5), demonstrating the high purity of the DLC samples and their stability as molecular

semiconductor materials. Furthermore, **5** and **6** show no charge carrier mobility rate electric-field dependence, an important feature for utilization of mesophase semiconductors.

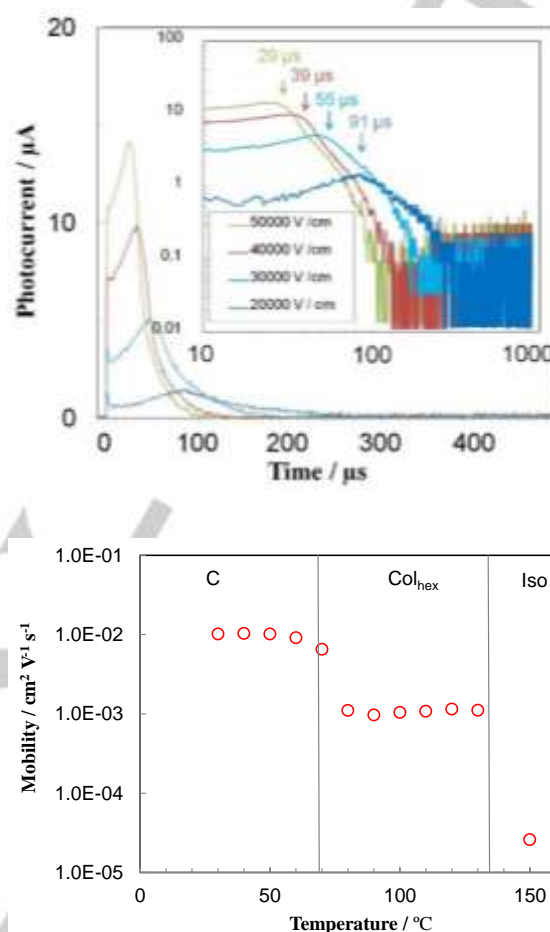


**Figure 4.** Model charge carrier mobility of **5** measured by time-of-flight (TOF). Electric field dependency of photocurrent curves for **5** at 120°C in the Col<sub>hex</sub> phase, cell thickness = 18.5  $\mu\text{m}$ . Temperature dependence of charge carrier mobility for hole (circle), measured on cooling from isotropic liquid.

For internal use, please do not delete. Submitted\_Manuscript

## FULL PAPER

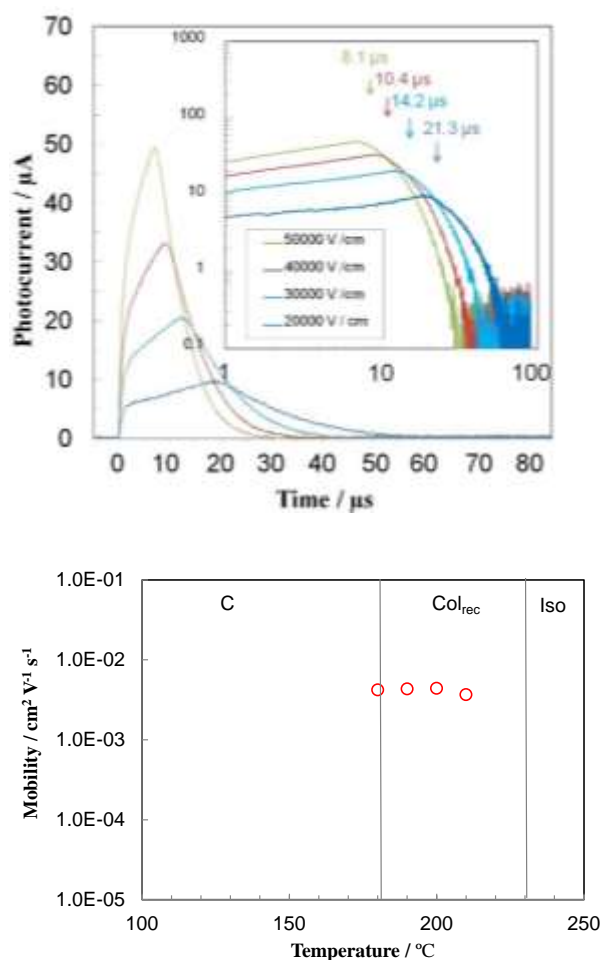


**Figure 5.** Model charge carrier mobility of **6** measured by time-of-flight (TOF). Electric field dependency of photocurrent curves for **6** at 200°C in the Col<sub>rec</sub> phase, cell thickness = 18.4 µm. Temperature dependence of charge carrier mobility for hole (circle), measured on cooling from isotropic liquid.

Compound **5**, which shows a moderate temperature range on heating, from 110 to ca 134°C but that extends to ca. 70°C on cooling, shows a low hole mobility rate of  $2.59 \times 10^{-5} \text{ cm}^2 \text{ V}^{-1} \text{ s}^{-1}$  at 150°C in the isotropic liquid phase. This value jumps up to  $1.15 \times 10^{-3} \text{ cm}^2 \text{ V}^{-1} \text{ s}^{-1}$  at 120°C in the Col<sub>hex</sub> mesophase, and rises up further to  $0.01 \text{ cm}^2 \text{ V}^{-1} \text{ s}^{-1}$  on cooling down to the meta-stable Col<sub>hex</sub> crystalline phase. The behavior of the electronic charge carrier mobility matches well the temperature dependency of the molecules dynamics and the order degree of molecular semiconductors (as supported by DSC). It is stressed that until the ambient temperature, **5** still shows non-dispersive photocurrent decay curves and the hole drift mobility can be measured, though the POM textures (Figure S26) display different domain boundaries begin to form.

Compound **6**, which displays a Col<sub>rec</sub> mesophase also with a moderate temperature range (40-50°C) and at much higher temperature than **5**, shows a hole mobility rate of  $3.78 \times 10^{-3} \text{ cm}^2 \text{ V}^{-1} \text{ s}^{-1}$  at 200°C on heating, while on cooling from the isotropic liquid to 200°C, the hole mobility rate is slightly increased to 4.39

$\times 10^{-3} \text{ cm}^2 \text{ V}^{-1} \text{ s}^{-1}$ . The hole mobility rate jumps to  $0.03 \text{ cm}^2 \text{ V}^{-1} \text{ s}^{-1}$  when it is cooled below 170°C (crystalline Col<sub>rec</sub> phase). On further cooling, highly dispersive photocurrent decay curves appear due to the crystalline grain boundaries playing the role of deep traps for charge carriers, and no accurate mobility value can be measured.

From the above TOF charge carrier mobility investigation, it can be concluded that these novel electron-rich thiophene-fused discotic columnar mesogens are stable, applicable p-type organic semiconductors. Both the ordered Col<sub>hex</sub> (discogen **5**) and Col<sub>rec</sub> (discotic dimer **6**) mesophases exhibit moderate hole mobility rate in range of  $10^{-3} \text{ cm}^2 \text{ V}^{-1} \text{ s}^{-1}$ . More interestingly, the meta-stable columnar crystalline phases show higher hole mobility with value in the  $10^{-2} \text{ cm}^2 \text{ V}^{-1} \text{ s}^{-1}$  range. Furthermore, compound **5**, with a twisted aromatic core, forms crystalline thin films without grain boundaries, which are suitable for charge hopping at ambient temperature. The planar molecule **6** exhibits narrow mesophase range and prefers to crystallize into small domains with grain boundaries that act as deep electronic traps.

DFT calculations revealed that the most-stable structures of these thiophene-fused molecules are in nearly co-planar conformation, benefiting optimized  $\pi$ - $\pi$  face-to-face stacking and columnar arrangement. The calculated HOMO and LUMO locate continuously along the linear fused-thiophene-containing polycyclic aromatic cores, implying favorable hole and electron hopping along the mesogenic columns. This study further reveal that it is possible to control electron mobility, as whilst **5** and **6** only show hole mobility, compound **7** shows both hole and electron mobilities.[38] These results of relationship between molecular geometry, mesomorphism, and semiconductivity might be a useful hint for further molecular design of discotic mesophase semiconductor.

**UV-vis absorption and Photoluminescence.** Discotic liquid crystalline compounds have great potential application in field of OLED and OPVs, their optical absorption and emission properties naturally arise our interests. The UV-Vis absorption spectra and photoluminescence in solution and as thin-films of **5-8** have been measured (Figure 6). The UV/Vis. absorption spectroscopy (Figure 6a) of fused thiophene aromatics **5-8** show series of peaks for each compound, the peaks with the longer wavelength come from the HOMO-LUMO excitation. The optical properties are coincident with the theoretical calculation results. As the  $\pi$ -conjugated aromatic systems gradually increased from **5** to **8**, their absorption peaks are red-shifting to longer wavelengths, in agreement with the gradual narrowing of the HOMO-LUMO energy gaps calculated for homologous methoxy derivatives **5'** to **8'** (Tables 3 and S1).

The photoluminescence spectra of **5-8** in solution (Figure 6b) display well resolved spectra with two intense peaks, and a shoulder for each compound, almost mirroring images of their respective absorption. However, their thin-film photoluminescent spectra (Figure 6c) are red-shifted to longer wavelength with only one peak. Thus, **5** and **7** are blue emitters, while **6** and **8** are greenish to reddish emitters. For thin-film emissions, the intermolecular  $\pi$ - $\pi$  stacking interactions result in strong  $\pi$ - $\pi$  orbital

For internal use, please do not delete. Submitted\_Manuscript

## FULL PAPER

overlap and thus band gaps are narrowed. The emission efficiency was measured in diluted solution. The absolute emitting quantum yield of **5** is quite low, only 2.04%, compared to the other compounds: QY of **6** increases to 10.68%, but more interestingly, QY of **7** and **8** display almost equal values, around 18%, a quite high value for a novel photoluminescent discogens. For these thiophene-fused aromatics, the QY increases with the  $\pi$ -conjugating system extending, while the reason for this result is not fully understood yet.

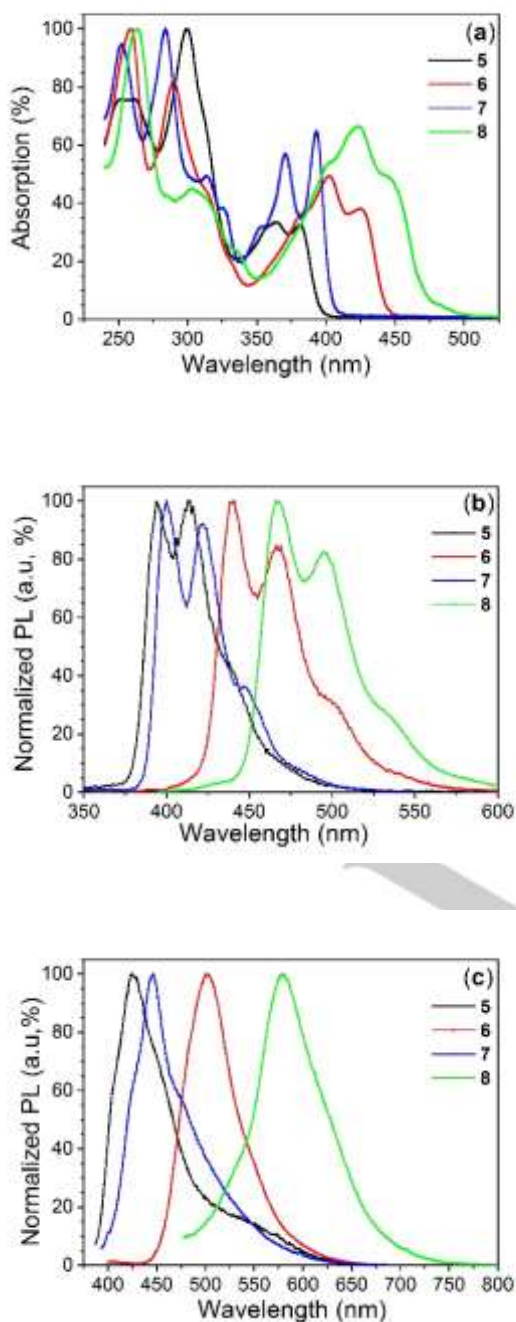


**Figure 6.** (a) Normalized absorption (in micromolar THF solution), (b) normalized emission in THF solution, and (c) normalized emission in thin film of **5-8** respectively.

**Table 3.** Photo-physical properties of fused thiophene aromatics.

Entry	$\lambda_{\text{abs}}^{[a]}$	$\epsilon^{[b]}$	$\lambda_{\text{em}}(\text{sol.})^{[c]}$	$\lambda_{\text{em}}(\text{film})^{[d]}$	Quantum yield <sup>[e]</sup>
<b>5</b>	257	$1.49 \times 10^5$	395	425	2.04
	300	$2.00 \times 10^5$			
	363	$6.68 \times 10^4$			
	382	$6.52 \times 10^4$			
<b>6</b>	258	$2.00 \times 10^5$	440	500	10.68
	290	$1.63 \times 10^5$			
	403	$9.88 \times 10^4$			
	425	$7.52 \times 10^4$			
<b>7</b>	252	$1.88 \times 10^5$	400	446	18.03
	283	$2.00 \times 10^5$			
	370	$1.13 \times 10^5$			
	393	$1.28 \times 10^5$			
<b>8</b>	262	$2.00 \times 10^5$	466	579	18.06
	303	$8.98 \times 10^4$			
	423	$1.33 \times 10^5$			

[a] Absorption ( $\lambda_{\text{abs}}$ ) and emission ( $\lambda_{\text{em}}$ ) wavelengths in nm; [b] Absorption coefficient,  $\epsilon$ , in  $\text{L mol}^{-1} \text{cm}^{-1}$ . [c] In micromolar THF solutions with solution concentration of  $5 \times 10^{-6} \text{ mol L}^{-1}$ . Excitation wavelength: 300 nm for **5**; 360 nm for **6**; 285 nm for **7**; 375 nm for **8**. [d] Prepared solution in THF. Excitation wavelength: 350 nm for **5**; 360 nm for **6**; 365 nm for **7**; 430 nm for **8**. [e] Quantum yields in % were measured with solution concentration of  $1 \times 10^{-4} \text{ mol L}^{-1}$  in THF excited at 310 nm (**5-8**).

## Conclusions

Several fused-thiophene discogens and two of their benzene analogues have been synthesized with high efficiency by Suzuki cross-coupling and tandem  $\text{FeCl}_3$  oxidized intra- and intermolecular Scholl reactions. The planar-cored compounds aggregate in organic solvents due to strong  $\pi$ - $\pi$  interactions, in contrast to the core-twisted compounds which do not show such a trend. All compounds nevertheless display thermotropic liquid crystalline properties, consisting essentially in the formation of  $\text{Col}_{\text{hex}}$  and  $\text{Col}_{\text{rec}}$  phases, for the fused and sigma-bridged dimers, respectively, whose supramolecular arrangements were comprehensively analyzed by POM, DSC, and SAXS. These new thiophene-containing discogens exhibit much lower phase transition temperatures than their benzene analogues, which is an important advantage for devices fabrication by solution or melting processing. Moreover, they behave as either blue, or greenish to reddish emitters, depending on the conjugation extension, with increasing QY, and two representatives of such thienoacene-based discogenic structures demonstrated fast hole mobility values, in the range  $10^{-3}$  and  $10^{-2} \text{ cm}^2 \text{ V}^{-1} \text{ s}^{-1}$ . Finally, the demonstration that the versatile synthetic strategy could be successfully extended to the synthesis of unsymmetrical discogens is of both fundamental and applied interests. For

For internal use, please do not delete. Submitted\_Manuscript

## FULL PAPER

instance, the preparation of Janus-type discogenic compounds, with two edges of different chemical natures can modify and adjust some properties, such as solubility, wettability, self-organization, phase transition temperatures, without altering the intrinsic electronic properties of the conjugated cores, and thus may represent a very practical tool to circumvent potential technological problems during their integration into electronic devices.

## Experimental Section

Experimental details are given in the supplementary information file.

## Acknowledgements

This work was financially supported by the National Natural Science Foundation of China (grant no. 21772135, 51773140) and a NSFC-JSPS joint project (grant no. 50811140156). BD and BH acknowledge CNRS and Université de Strasbourg for support.

**Keywords:** thiophene • charge mobility • luminescence • mesophase • cyclo-hydrogenation

- [1] T. Kato, M. Yoshio, T. Ichikawa, B. Soberats, H. Ohno, M. Funahashi, *Nat. Rev. Mater.* **2017**, *2*, 17001.
- [2] H. Iino, T. Usui, J. Hanna, *Nat. Commun.* **2015**, *6*, 6828.
- [3] I. McCulloch, M. Heeney, C. Bailey, K. Genevicius, I. MacDonald, M. Shkunov, D. Sparrowe, S. Tierney, R. Wagner, W. Zhang, M. L. Chabinyo, R. J. Kline, M. D. McGehee, M. F. Toney, *Nat. Mater.* **2006**, *5*, 328-333.
- [4] A. Matsui, M. Funahashi, T. Tsuji, T. Kato, *Chem. Eur. J.* **2010**, *16*, 13465-13472.
- [5] X. Crispin, F. L. E. Jakobsson, A. Crispin, P. C. M. Grim, P. Andersson, A. Volodin, C. van Haesendonck, M. Van der Auweraer, W. R. Salaneck, M. Berggren, *Chem. Mater.* **2006**, *18*, 4354-4360.
- [6] G. Zhao, Y. He, Y. Li, *Adv. Mater.* **2010**, *22*, 4355-4358.
- [7] H. Iino, J. Hanna, *Polym. J.* **2017**, *49*, 23-30.
- [8] J. Hanna, A. Ohno, H. Iino, *Thin Solid Films* **2014**, *554*, 58-63.
- [9] Y. Kim, M. Funahashi, N. Tamaoki, *RSC Adv.* **2014**, *4*, 60511-60518.
- [10] K. Lin, G. Lee, C. K. Lai, *Tetrahedron* **2015**, *71*, 4352-4361.
- [11] Q. Meng, X. Sun, Z. Lu, P. Xia, Z. Shi, D. Chen, M. Wong, S. Wakim, J. Lu, J. Baribeau, Y. Tao, *Chem. Eur. J.* **2009**, *15*, 3474-3487.
- [12] M. Melucci, L. Favaretto, C. Bettini, M. Gazzano, N. Camaioni, P. Maccagnani, P. Ostojica, M. Monari, G. Barbarella, *Chem. Eur. J.* **2007**, *13*, 10046-10054.
- [13] Y. Wang, H. Iino, J. Hanna, *Appl. Phys. Lett.* **2017**, *111*, 133301.
- [14] Y. Wang, H. Iino, J. Hanna, *Soft Matter* **2017**, *13*, 6499-6505.
- [15] M. C. McCairn, T. Kreouzis, M. L. Turner, *J. Mater. Chem.* **2010**, *20*, 1999-2006.
- [16] C. Niebel, Y. Kim, C. Ruzié, J. Karpinska, B. Chattopadhyay, G. Schweizer, A. Richard, V. Lemaury, Y. Olivier, J. Cornil, A. R. Kennedy, Y. Diao, W. Lee, S. Mannsfeld, Z. Bao, Y. H. Geerts, *J. Mater. Chem. C* **2015**, *3*, 674-685.
- [17] Y. Funatsu, A. Sonoda, M. Funahashi, *J. Mater. Chem. C* **2015**, *3*, 1982-1993.
- [18] T. Hamamoto, M. Funahashi, *J. Mater. Chem. C* **2015**, *3*, 6891-6900.
- [19] L. Mazur, A. Castiglione, K. Ocytko, F. Kameche, R. Macabies, A. Aïnsebaa, D. Kreher, B. Heinrich, B. Donnio, S. Sanaur, E. Lacaze, J. Fave, K. Matczyszyn, M. S. Jeong, W. Wu, A. Attias, Jean. Ribierre, F. Mathevet, *Org. Electron.* **2014**, *15*, 943-953.
- [20] F. Lincker, B. Heinrich, R. D. Bettignies, P. Rannou, J. Pécaut, B. Grévin, A. Pron, B. Donnio, R. Demadrille, *J. Mater. Chem.* **2011**, *21*, 5238-5247.
- [21] H. Wu, H. Iino, J. Hanna, *RSC Adv.* **2017**, *7*, 56586-56593.
- [22] A. J. J. M. van Breemen, P. T. Herwig, C. H. T. Chlon, J. Sweelssen, H. F. M. Schoo, S. Setayesh, W. M. Hardeman, C. A. Martin, D. M. de Leeuw, J. J. P. Valetton, C. W. M. Bastiaansen, D. J. Broer, A. R. Popa-Merticar, S. C. J. Meskers, *J. Am. Chem. Soc.* **2006**, *128*, 2336-2345.
- [23] K. Oikawa, H. Monobe, K. Nakayama, T. Kimoto, K. Tsuchiya, B. Heinrich, D. Guillon, Y. Shimizu, M. Yokoyama, *Adv. Mater.* **2007**, *19*, 1864-1868.
- [24] H. Monobe, L. An, P. Hu, B. Wang, K. Zhao, Y. Shimizu, *Mol. Cryst. Liq. Cryst.* **2017**, *647*, 119-126.
- [25] Y. Shimizu, K. Oikawa, K. Nakayama, D. Guillon, *J. Mater. Chem.* **2007**, *17*, 4223-4229.
- [26] S. Sergeyev, W. Pisulab, Y. H. Geerts, *Chem. Soc. Rev.* **2007**, *36*, 1902-1929.
- [27] T. Wöhrle, I. Wurzbach, J. Kirres, A. Kostidou, N. Kapernaum, J. Litterscheidt, J. C. Haenle, P. Staffeld, A. Baro, F. Giesselmann, S. Laschat, *Chem. Rev.* **2016**, *116*, 1139-1241.
- [28] K. Zhao, C. Chen, H. Monobe, P. Hu, B. Wang, Y. Shimizu, *Chem. Commun.* **2011**, *47*, 6290-6292.
- [29] H. Ni, H. Monobe, P. Hu, B. Wang, Y. Shimizu, K. Zhao, *Liq. Cryst.* **2013**, *40*, 411-420.
- [30] J. Luo, B. Zhao, J. Shao, K. A. Lim, H. S. O. Chana, C. Chi, *J. Mater. Chem.* **2009**, *19*, 8327-8334.
- [31] J. Luo, B. Zhao, H. S. O. Chana, C. Chi, *J. Mater. Chem.* **2010**, *20*, 1932-1941.
- [32] E. Miyazaki, A. Kaku, H. Mori, M. Iwatania, K. Takimiya, *J. Mater. Chem.* **2009**, *19*, 5913-5915.
- [33] A. D. Bromby, W. H. Kana, T. C. Sutherland, *J. Mater. Chem.* **2012**, *22*, 20611-20617.
- [34] L. Zhang, D. L. Hughes, A. N. Cammidge, *J. Org. Chem.* **2012**, *77*, 4288-4297.
- [35] S. K. Maier, S. S. Jester, U. Müller, W. M. Müllera, S. Höger, *Chem. Commun.* **2011**, *47*, 11023-11025.
- [36] S. Méry, D. Haristoy, J. Nicoud, D. Guillon, S. Diele, H. Monobe, Y. Shimizu, *J. Mater. Chem.* **2002**, *12*, 37-41.
- [37] D. Tian, Y. Zhou, Z. Li, S. Liu, J. Shao, X. Yang, J. Shao, W. Huang, B. Zhao, *ChemistrySelect* **2017**, *2*, 8137-8145.
- [38] C. Liu, H. Wang, J. Du, K. Zhao, P. Hu, B. Wang, H. Monobe, B. Heinrich, B. Donnio, *J. Mater. Chem. C* **2018**, *6*, 4471-4478.
- [39] T. Yasuda, H. Ooi, J. Morita, Y. Akama, K. Minoura, M. Funahashi, T. Shimomura, T. Kato, *Adv. Funct. Mater.* **2009**, *19*, 411-419.
- [40] T. Yasuda, T. Shimizu, F. Liu, G. Ungar, T. Kato, *J. Am. Chem. Soc.* **2011**, *133*, 13437-13444.
- [41] L. Chen, S. R. Puniredd, Y. Tan, M. Baumgarten, U. Zschieschang, V. Enkelmann, W. Pisula, X. Feng, H. Klauk, K. Müllen, *J. Am. Chem. Soc.* **2012**, *134*, 17869-17872.
- [42] Q. Xiao, T. Sakurai, T. Fukino, K. Akaike, Y. Honsho, A. Saeki, S. Seki, K. Kato, M. Takata, T. Aida, *J. Am. Chem. Soc.* **2013**, *135*, 18268-18271.
- [43] A. Demenev, S. H. Eichhorn, T. Taerum, D. F. Perepichka, S. Patwardhan, F. C. Grozema, L. D. A. Siebbeles, R. Klenker, *Chem. Mater.* **2010**, *22*, 1420-1428.
- [44] M. Mitani, S. Ogata, S. Yamane, M. Yoshio, M. Hasegawa, T. Kato, *J. Mater. Chem. C* **2016**, *4*, 2752-2760.
- [45] K. P. Gan, M. Yoshio, T. Kato, *J. Mater. Chem. C* **2016**, *4*, 5073-5080.
- [46] A. Casey, Y. Han, M. F. Wyatt, T. D. Anthopoulos, M. Heeney, *RSC Adv.* **2015**, *5*, 90645-90650.
- [47] K. Zhao, J. Du, X. Long, M. Jing, B. Wang, P. Hu, H. Monobe, B. Heinrich, B. Donnio, *Dyes Pigm.* **2017**, *143*, 252-260.
- [48] M. C. Artal, K. J. Toyne, J. W. Goodby, J. Barbera, D. J. Photinos, *J. Mater. Chem.* **2001**, *11*, 2801-2807.

For internal use, please do not delete. Submitted\_Manuscript

## FULL PAPER

- [49] D. Mysliwiec, B. Donnio, P. J. Chmielewski, B. Heinrich, M. Stepien, *J. Am. Chem. Soc.* **2012**, *134*, 4822-4833.
- [50] B. Alameddine, O. F. Aebischer, B. Heinrich, D. Guillon, B. Donnio, T. A. Jenny, *Supramol. Chem.* **2014**, *26*, 125-137.
- [51] Y. Yang, H. Wang, H. Wang, C. Liu, K. Zhao, B. Wang, P. Hu, H. Monobe, B. Heinrich, B. Donnio, *Cryst. Growth Des.* **2018**, *18*, 4296-4305.
- [52] K. Zhao, M. Jing, L. An, J. Du, Y. Wang, P. Hu, B. Wang, H. Monobe, B. Heinrich, B. Donnio, *J. Mater. Chem. C* **2017**, *5*, 669-682.
- [53] K. Zhao, Y. Gao, W. Yu, P. Hu, B. Wang, B. Heinrich, B. Donnio, *Eur. J. Org. Chem.* **2016**, *2016*, 2802-2814.
- [54] K. Zhao, X. Bai, B. Xiao, Y. Gao, P. Hu, B. Wang, Q. Zeng, C. Wang, B. Heinrich, B. Donnio, *J. Mater. Chem. C* **2015**, *3*, 11735-11746.
- [55] K. Zhao, L. An, X. Zhang, W. Yu, P. Hu, B. Wang, J. Xu, Q. Zeng, H. Monobe, Y. Shimizu, B. Heinrich, B. Donnio, *Chem. Eur. J.* **2015**, *21*, 10379-10390.
- [56] L. Schmidt-Mende, A. Fechtenkötter, K. Müllen, E. Moons, R. H. Friend, J. D. MacKenzie, *Science* **2001**, *293*, 1119-1122.

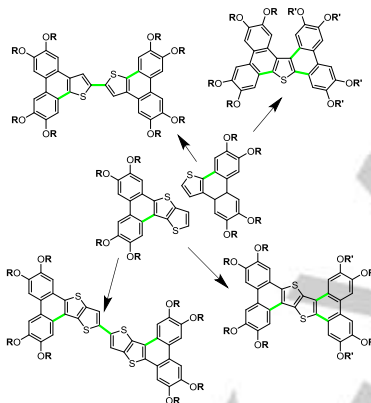
## FULL PAPER

## Entry for the Table of Contents (Please choose one layout)

Layout 1:

## FULL PAPER

Tandem  $\text{FeCl}_3$  oxidized intra- and intermolecular Scholl reactions applied to the fabrication of discotic mesogens, with tunable color-emission and fast charge carriers



Kai-Chun Zhao, Jun-Qi Du, Hai-Feng Wang, Ke-Qing Zhao, \* Ping Hu, Bi-Qin Wang, Hirosato Monobe, \* Benoît Heinrich and Bertrand Donnio\*

Page No. – Page No.

**Board-like Fused-Thiophene Liquid Crystals and Their Benzene Analogues: Facile Synthesis, Self-assembly, p-Type Semiconductivity, and Photoluminescence**